(Received 4 February 2024, Accepted 14 March 2024, Scheduled 30 March 2024)

Research on Resonant Wireless Energy Supply Circular Reactive Shielding for Small Electronic Equipment

Jishen Peng, Sylla Tidiani, Heyi Cao*, Yuepeng Liu, and Weihua Chen

Faculty of Electrical and Control Engineering, Liaoning Technology University, Huludao 125000, China

ABSTRACT: A reactive power shielding structure working under 150 kHz for small electronic equipment was proposed to reduce the electromagnetic leakage of WPT system. First, the model of LCC-LCC compensation circuit was established. By ensuring transmission efficiency, a comprehensive analysis of nine sets of computational data results was conducted to select the scheme with the best shielding effect. The experimental results showed that the magnetic flux density attenuation was 27.82% at 41 mm transmission distance from the center under the optimal structure of 3 rings and 7 turns, inner diameter of 23 mm, and outer diameter of 35 mm. The transmission efficiency can reach 76.73%, which is only 1.32% lower than the situation without shielding. The proposed reactive power shielding structure can significantly reduce the magnetic flux density in the external area of the WPT system without affecting the transmission efficiency of the system.

1. INTRODUCTION

Along with the continuous development of electronic technology, wireless power transfer technology has gradually become a popular research focus. Wireless power transfer (WPT) system is widely applied in various fields such as the powering of implantable devices, electronic equipment, and smart homes [1–7]. When powering small electronic devices, the gap between the receiving coil and transmitting coil of the WPT system leads to magnetic field leaking out of the working area, adversely causing negative effect on the system's transmission efficiency and electromagnetic environment. Therefore, global scholars have conducted extensive research on the crucial researching focuses of enhancing transmission efficiency and reducing electromagnetic leakage.

Magnetic field shielding can be classified as material shielding [8–13] and coil shielding for material shielding, and the high conductivity of copper and aluminum metal plates will lead to eddy current losses, significantly reducing system efficiency. Adopting high permeability low-loss ferrite materials can enhance the system's performance and reduce the magnetic field leakage between systems. However, flaws of ferrite materials including high cost, being heavy and fragile make them unsuitable for magnetic field leakage shielding of small devices. Electromagnetic metamaterials can also be applied in WPT systems for improving transmission efficiency and reducing electromagnetic field (EMF) leakage in MHz frequency range. However, metamaterial slabs applied in WPT systems are mainly based on printed circuit board (PCB) technique, which causes heavy trace losses in kHz range, rendering metamaterial characteristics somewhat insignificant.

Coil shielding can be classified into active shielding and passive shielding. Campi et al. conducted research on active shielding and proposed a novel active coil shielding design. The traditional active loop for shielding was divided into two separate shielding coils to avoid adverse effect on WPT performance. Experimental results showed a significant magnetic field strength reduction in the target shielding area. However, the efficiency of the WPT system is slightly reduced in the proposed design [14]. Active shielding allows precise control of the shielding coil to generate magnetic field in the opposite direction of magnetic field leakage by applying external excitation, therefore effectively suppressing electromagnetic leakage. However, when the shielding coil is involved in the main magnetic circuit, it will couple with the receiving or transmitting coils, leading to reduction in the system coupling coefficient, subsequently affecting transmission efficiency. Additionally, active shielding faces problems such as high expense and complex operation process. Non-resonant reactive shielding can reduce peripheral EMF leakage levels at the cost of decreased efficiency [15–20]. Park et al. conducted research on resonant reactive shielding by placing closed-loop shielding coils with matching capacitors around the receiving or transmitting coils. The system's leaked magnetic field was collected as the excitation for the shielding coil to generate a counteracting magnetic field. Matching capacitors are used to adjust the phase and magnitude of the shielding coil current to achieve optimized shielding effects [21]. Research on multi-coil circular resonant reactive shielding structures can be consequently undertaken, which can significantly reduce the magnetic field in the external region of the WPT system without affecting the system's transmission efficiency and reactive power.

In this paper, we propose a reactive shielding structure suitable for small electronic devices under 150 kHz resonant frequency. First, a coil model was established, and parameters are optimized based on the model. The annular shielding coil is positioned on the outer side parallel to the main coil. The current

* Corresponding author: Heyi Cao (18342986383@163.com).

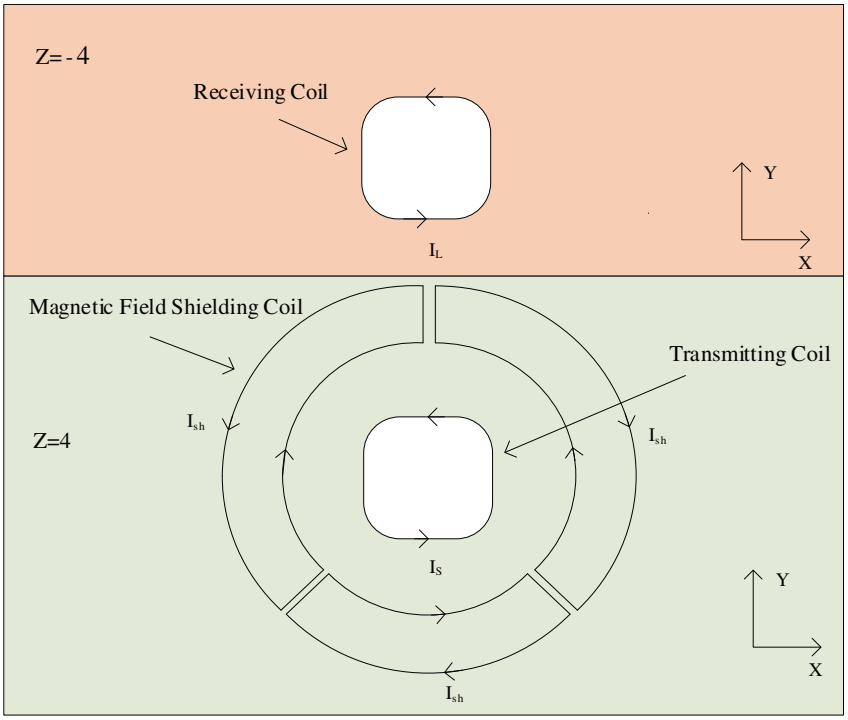

FIGURE 1. Three-loop reactive power shielding structure.

direction on the inner side of the shielding coil is consistent with the main coil's current direction, generating a magnetic field in the same direction to ensure system transmission efficiency. The current direction on the outer side of the shielding coil is opposite to the main coil's current direction, producing a reverse magnetic field to shield electromagnetic leakage at the transmission end's periphery. By adjusting the matching capacitor in the shielding coil, the magnitude and phase of the shielding coil current can be regulated to optimize the shielding effect.

2. THE WORKING PRINCIPLE OF THE ANNULAR REACTIVE SHIELDING COIL

2.1. The Design and Shielding Principle of the Annular Reactive Shielding Coil

The reactive shielding structure we proposed is as shown in Figure 1. Multiple annular coils are placed in parallel around the main coil. The analysis focuses on the shielding coil structure with three annular routes. The structural and electrical characteristics of the three shielding coils are the same. All shielding coils are separately equipped with matching capacitors to form a resonant reactive shielding structure.

The magnetic field generated by the WPT system is solely determined by the sum of the receiving and transmitting coils in the WPT structure without shielding structure. The loose coupling between the transmitting and receiving coils in the WPT system leads to the magnetic field leakage into non-working areas, adversely affecting both the system's transmission efficiency and electromagnetic environment. With the shielding structure applied in the WPT system, the total magnetic field produced by the system is the result of the superposition of the magnetic field generated by the receiving coil, transmitting coil, and shielding coil. The basic principle of resonant annular reactive shielding is introduced as follows. The leaked magnetic field from the transmission coil is utilized by the shielding annular coils as excitation source to induce voltage and current. By adjusting the matching capacitor, the magnitude and phase of the shielding current are controlled to achieve the optimal shielding effect. A magnetic field in the same direction of transmission coil is generated on the inner side of shielding coil to ensure the system's transmission efficiency, whereas a reverse magnetic field is generated on the outer side of the shielding coil to reduce the level of peripheral EMF leakage.

The cross-sectional view of the magnetic field generated by the WPT system and its leakage without the presence of shielding coils is as shown in Figure 2. Figure 3 is the cross-sectional illustration of the magnetic field generated by the WPT system after incorporating resonant reactive shielding coils and the cross-sectional representation of the shielding current direction.

The proposed resonant reactive shielding design involves the use of PCB material for the fabrication of shielding coils because of the effective reduction of spatial requirements and ease of secure positioning characteristics of PCB slabs. Annular reactive shielding coils are strategically placed on the outer side of the transmitting coil, with matching capacitors positioned on the back of the PCB, collectively forming a resonant structure. For the efficiency reduction caused by the gap between the transmission and receiving coils in the near field coupling process of the WPT system, we optimized the coil parameters to effectively enhance system transmission efficiency. For the 3-

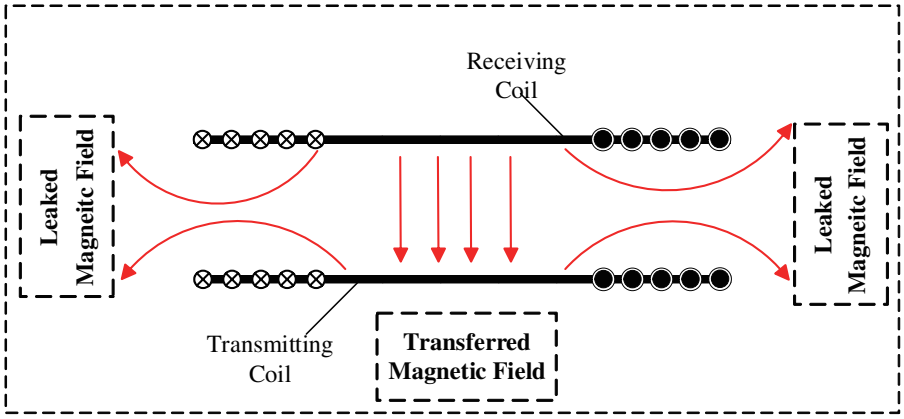

FIGURE 2. Cross-sectional view of the magnetic field generated by the transmission coil.

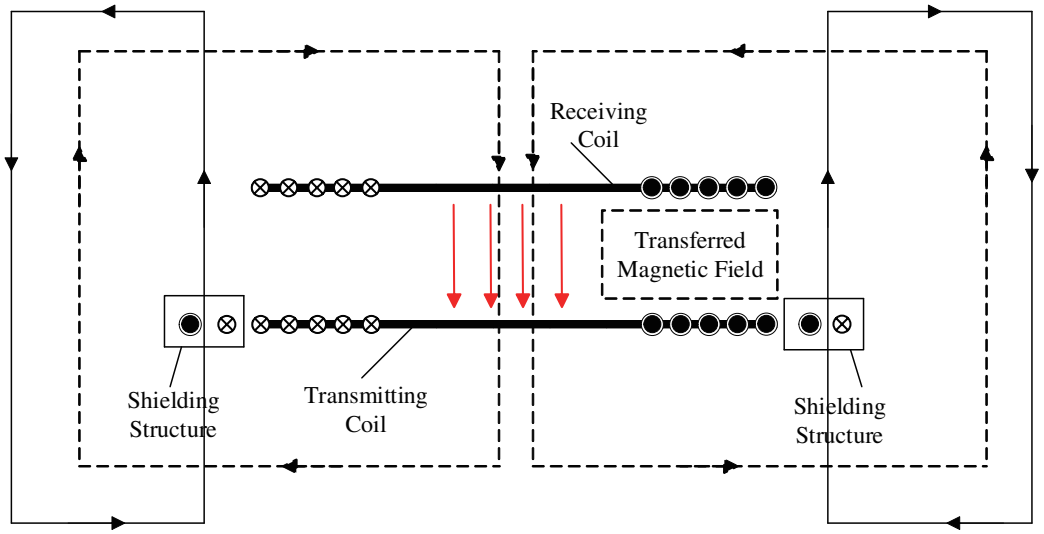

FIGURE 3. Cross-sectional view of the magnetic field generated by the resonant reactance shielding coil.

ring shielding coils, considering different numbers of turns and varying annular areas, a comparative analysis is conducted for system transmission efficiency and peripheral EMF leakage under various conditions. The optimal parameters of the shielding coils are acquired based on the comparison results to minimize peripheral EMF leakage and ensure optimal transmission efficiency for the WPT system, simultaneously. We established an experimental platform for the WPT system with shielding coils and analyzed the impact of different shielding coils on system transmission efficiency and peripheral magnetic field leakage through experimental analysis.

2.2. Analysis of Reactive Shielding Ring Coil Principle

Resonant reactive power shielding structure consists of three groups of identically structured and electrically characterized annular shielding coil sets. Each set of annular shielding coils can adjust its impedance by modifying its own matching capacitor, thereby controlling the magnitude and phase of the shielding current. The magnitude and phase of the shielding current determine the system's transmission efficiency and electromagnetic shielding effect. Hence, the impedance of the shielding coils is a crucial part of the design. Figure 4 shows the equivalent circuit model of the WPT system with shielding coils. Figure 5 illustrates the equivalent model of the shielding coil.

The resonant reactive shielding structure consists of three sets of annular shielding coils. Figure 5 illustrates the structure composed of a single shielding coil. Each set of annular shielding coils collects the leaked magnetic field during near-field coupling of the WPT system as excitation source (V). $\mathbf{I}_{\mathrm{p}}$, $\mathbf{I}_{\mathrm{s}}$, $\mathbf{I}_{\mathrm{sh1}}$, $\mathbf{I}_{\mathrm{sh2}}$, and $\mathbf{I}_{\mathrm{sh3}}$ are the currents in the transmitting and receiving circuits; the 3-ring shielding coils' L_{sh1} is the shielding coil inductance; R_{sh1} is the parasitic resistance; and C_{sh1} is the total capacitance of matching capacitor and parasitic capacitance of the shielding coil. The impedance of the shielding coil circuit can be modified by adjusting the capacitance of the matching capacitor to control the magnitude and phase of the shielding coil current, thus weakening the total magnetic field of the WPT system. In WPT system with shielding structure, the main coil is a symmetric structure, and the shielding coils are placed around the main coil in a parallel and symmetrical manner. Therefore, the currents in the three sets of shielding

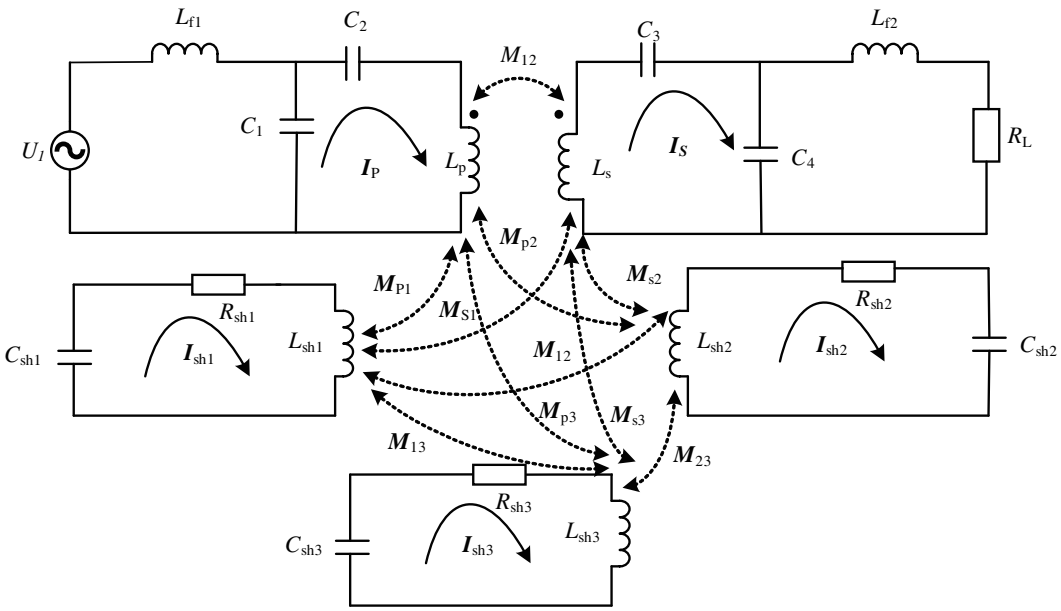

FIGURE 4. Equivalent circuit of resonant reactive power shielded WPT system.

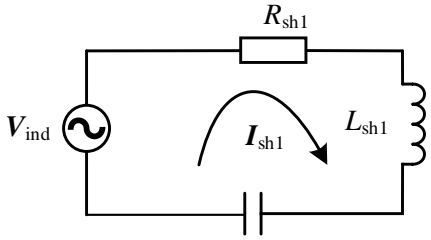

FIGURE 5. Equivalent model of shielding coil.

coils have the same expression. The following analysis is based on the circuit of one shielding coil.

When the incident magnetic field of the WPT system passes through the resonant reactive shielding coil, the induced voltage $\mathbf{V}_{\text{ind}}$ on the shielding coil can be expressed as:

$$\mathbf{V}_{\text{ind}} = -\frac{\mathrm{d}\phi}{\mathrm{d}t} = -\mathrm{j}\omega\,\mathbf{B}_0\,\mathrm{e}^{\mathrm{j}\omega t}\cdot\mathbf{S} \tag{1}$$

where ω is the angular frequency of the WPT system, $\boldsymbol{S}$ the area of a single shielding coil loop, and $\mathbf{B}_0$ the total magnetic induction entering a single shielding coil.

The phase of the shielding coil impedance varies according to frequency change. When the system operating frequency is higher than the resonant frequency of the shielding coil, the phase of the impedance is approximately 90°. At this point, the inductive impedance of the shielding coil is greater than the capacitive impedance. The shielding coils exhibit inductive impedance, resulting in a phase angle opposite to the original magnetic field, thus achieving the shielding effect. When the system operating frequency is lower than the resonant frequency of the shielding coil, the phase of the impedance is approximately −90°. At this point, the capacitive impedance of the shielding coil is greater than the inductive impedance, exhibiting a capacitive impedance. This produces a phase angle identical to the original magnetic field. In this case, not only does it not weaken the total magnetic field of the WPT system, but also it may increase its EMF leakage level. Therefore, the shielding impedance should be designed in the inductive region, where the resonant frequency is lower than the system operating frequency. The shielding current is expressed as:

$$\mathbf{I}_{\text{sh}} = \frac{\mathbf{V}_{\text{ind}}}{Z_{\text{sh}}} = \frac{\mathbf{V}_{\text{ind}}}{\mathrm{j}\omega\,L_{\text{sh}} + \frac{1}{\mathrm{j}\omega\,C_{\text{sh}}} + R_{\text{sh}}} \tag{2}$$

where Z_{sh} is the equivalent impedance of the shielding coil, L_{sh} the self-inductance of the shielding coil, C_{sh} the resonant capacitance of the shielding coil, and R_{sh} the equivalent parasitic resistance of the shielding coil.

When the shielding coil operates in the inductive region, as the inductive impedance of the shielding coil is greater than the capacitive impedance, the system frequency is higher than the resonant frequency of the shielding coil. At this point, the shielding current can be expressed as:

$$\frac{1}{\mathrm{j}\omega\,C_{\text{sh}}} < \mathrm{j}\omega\,L_{\text{sh}} \tag{3}$$

$$\mathbf{I}_{\text{sh}} = \frac{\mathbf{V}_{\text{ind}}}{\mathrm{j}\omega\,L_{\text{eq}} + R_{\text{sh}}} \tag{4}$$

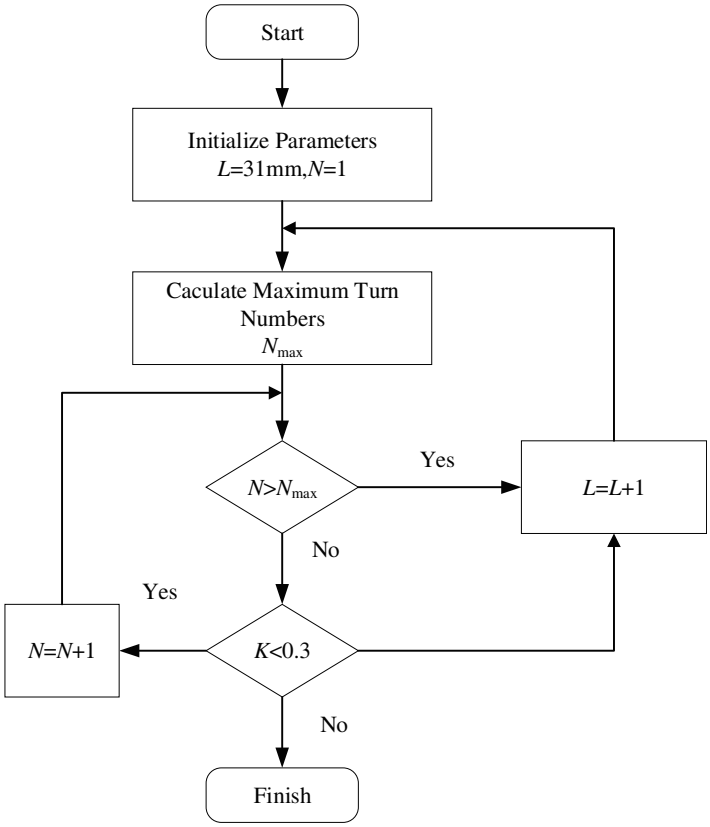

FIGURE 6. Flowchart of main coil design.

The expression for the equivalent inductance L_{eq} of the shielding coil is shown as follows:

$$L_{eq} = \left(L_{sh} - \frac{1}{\omega^2 C_{sh}}\right) \tag{5}$$

The resonant multi-coil annular reactive shielding, taking a single-loop shielding coil as an example, is analyzed for its working principle. According to Kirchhoff's Voltage Law (KVL), we have:

$$\begin{aligned} &\frac{\mathbf{U}_1\left(C_1 + C_2 - \omega^2 L_p C_1 C_2\right)}{C_2} \\ &= \left(\mathrm{j}\omega L_{fl} - \mathrm{j}\omega^3 L_{fl} L_p C_1 + \mathrm{j}\omega L_p + \frac{1 - \omega^2 L_{fl} C_1}{\mathrm{j}\omega C_2}\right)\mathbf{I}_{fl} \\ &\quad -\mathrm{j}\omega M_{sp}\mathbf{I}_s + \mathrm{j}\omega M_{p1}\mathbf{I}_{sh1} \end{aligned} \tag{6}$$

$$0 = \left(\frac{\mathrm{j}\omega L_{f2} + R_L}{1 - \omega^2 L_{f2} C_4 + \mathrm{j}\omega C_4 R_L} + \frac{1}{\mathrm{j}\omega C_3} + \mathrm{j}\omega L_s\right)\mathbf{I}_s - \mathrm{j}\omega M_{sp}\mathbf{I}_p - \mathrm{j}\omega M_{s1}\mathbf{I}_{sh1} \tag{7}$$

$$0 = \left(R_{sh1} + \mathrm{j}\omega L_{sh1} + \frac{1}{\mathrm{j}\omega C_{sh1}}\right)\mathbf{I}_{sh} + \mathrm{j}\omega M_{p1}\mathbf{I}_p - \mathrm{j}\omega M_{s1}\mathbf{I}_s \tag{8}$$

From (6)–(8), we can acquire the input current, calculate the input power P_{in} and output power P_{out} flowing through the load resistance R_L, and then calculate the system transmission efficiency η.

$$\eta = \frac{P_{out}}{P_{in}} \tag{9}$$

2.3. Design of Reactive Shielding Annular Coil Parameter

2.3.1. Main Coil Design

The main coil is made of copper wire with a diameter A of 0.3 mm, closely wound with no spacing d between turns, and the transmission distance is set as 8 mm. Due to the design placing the shielding coil parallel to the outer side of the rounded square main coil, certain constraints are imposed on the outer diameter L, inner diameter H, number of turns N, and coupling coefficient K of the main coil. The design process for the main coil is illustrated in Figure 6.

The circular square main coil is modeled by finite element simulation software COMSOL Multiphysics. A parametric scan is conducted on different outer diameters L and numbers of turns N to find the optimal values for the coupling coefficient, considering the constraints. The results of parametric scan are shown in Figure 7. The results show that the system's coupling coefficient reaches its highest value of 0.3120 when the outer diameter of the main coil is 34 mm, and the number of turns is 26. At this point, the simulated self-inductance of the main coil is 23 μH.

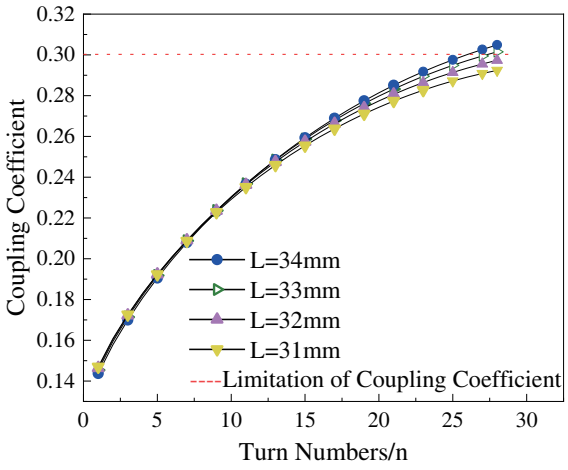

FIGURE 7. Simulation results of the main coil.

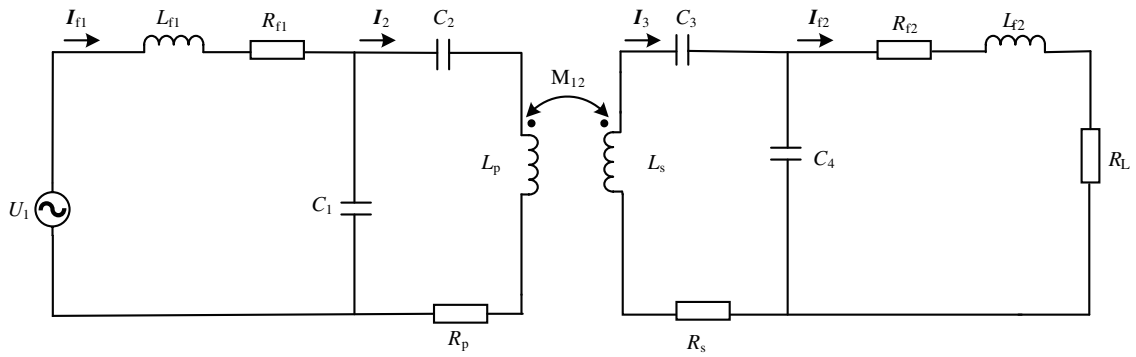

FIGURE 8. Equivalent circuit based on LCC-LCC compensation topology.

2.3.2. Determining the Optimal Value for p

Figure 8 shows the equivalent circuit model of the LCC-LCC compensation topology. U_1 represents the AC voltage source, where L_p and L_s are the self-inductances of the receiving and transmitting coils, respectively. L_{f1} and L_{f2} are series-compensating inductances on the primary and secondary sides, while C_1 and C_4 are parallel-compensating capacitors on the primary and secondary sides. C_2 and C_3 are series-compensating capacitors on the primary and secondary sides. R_{f1} and R_{f2} are the series internal resistances of the primary and secondary inductances, and R_p and R_S represent the internal resistances of the main coil. R_L is the load resistance. The model takes the influence of the internal resistance of compensating inductances on the system's transmission efficiency in account.

In this paper, the system input impedance is purely resistive under 150 kHz resonant frequency. Thus, the resonance equation is satisfied by:

$$\begin{cases} \omega^2 L_{f1} C_1 = 1 \\ \omega^2 \left(L_p - L_{f1}\right) C_2 = 1 \\ \omega^2 L_{f2} C_4 = 1 \\ \omega^2 \left(L_s - L_{f2}\right) C_3 = 1 \end{cases} \tag{10}$$

As the LCC-LCC resonance formula shows, $L_{f1}\,C_1$ and $L_{f2}\,C_4$ only satisfy a product relationship at 150 kHz resonance frequency. The specific parameters of the compensation inductance and compensation capacitance cannot be determined through the resonance formula alone. Therefore, the ratio of the compensation inductance to the main coil inductance is defined as P. Through the construction of an LCC-LCC simulation circuit in the MATLAB SIMULINK module, the simulation includes setting the self-inductance, mutual inductance, and other parameters of the main coil, obtained from the simulation in Subsection 2.1. Performing a parametric scan on P in the range of 0.01 to 0.99, Figure 9 displays the varying system transmission efficiency corresponding to different P values. The optimal system transmission efficiency is achieved when the ratio of compensation inductance to main coil inductance is 0.33. The specific parameters for the compensation at this point are determined for the system.

3. SIMULATION VERIFICATION OF REACTIVE SHIELDING TOROIDAL COIL

3.1. Simulation Settings

A model of a 3-loop shielding coil is constructed in multi-physics. The working frequency of the WPT system is set to 150 kHz, and the resonant frequency of the shielding coil is set

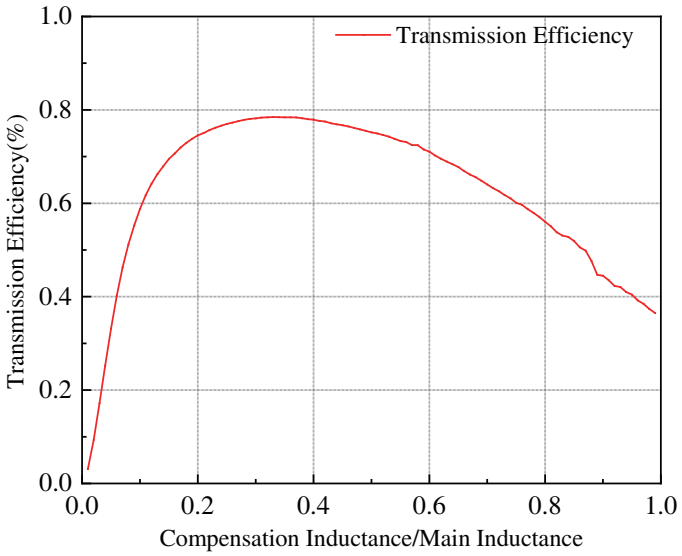

FIGURE 9. Effect of inductance ratio on system transmission efficiency.

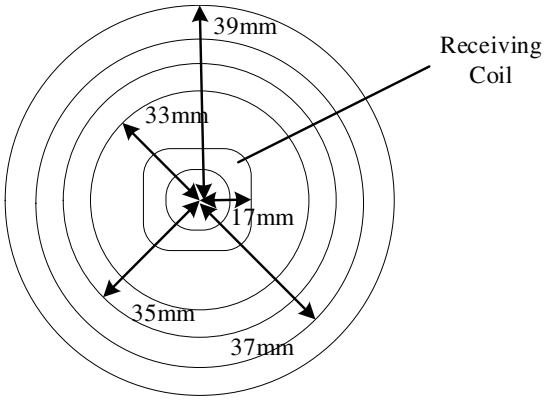

FIGURE 10. Magnetic field measurement points.

TABLE 1. Parameters of WPT main coil and shield coil.

Parameters	Loop number	Side length/mm	Turn numbers	Wire thickness/mm	Transmission distance/mm
Tx		34	26	0.3	
Rx		34	26	0.3	8
Shielding coil	3	Outer 35, inner 23, 24, 25	5, 7, 9	0.3	

TABLE 2. Simulation design schemes of different shielded coils.

Set No.	Loop number	Turn number	Outer diameter/mm	Inner diameter/mm
0	No shielding	No shielding	No shielding	No shielding
1	3 loops	5	35	23
2	3 loops	5	35	24
3	3 loops	5	35	25
4	3 loops	7	35	23
5	3 loops	7	35	24
6	3 loops	7	35	25
7	3 loops	9	35	23
8	3 loops	9	35	24
9	3 loops	9	35	25

to 145 kHz. As the shielding current is related to the number of turns N and the loop area S of the shielding circuit, nine different configurations of 3-loop shielding coils with varying numbers of turns and loop areas are designed in this paper. The analysis explores the impact of different shielding coils on the system's transmission efficiency and peripheral magnetic flux density.

The magnetic field measurement points are located on concentric circles in the same plane as the receiving end. Four concentric circles are chosen with radii $R_1 = 33$ mm, $R_2 = 35$ mm, $R_3 = 37$ mm, and $R_4 = 39$ mm, as illustrated in Figure 10.

The simulation parameters and design schemes for the shielding coils with different numbers of turns and loop areas are presented in Table 1 and Table 2.

3.2. Simulation Analysis

The simulation results for the 10 shielding schemes are shown in Figure 11. Each shielding scheme effectively weakens the total magnetic field of the WPT system, reducing electromag-

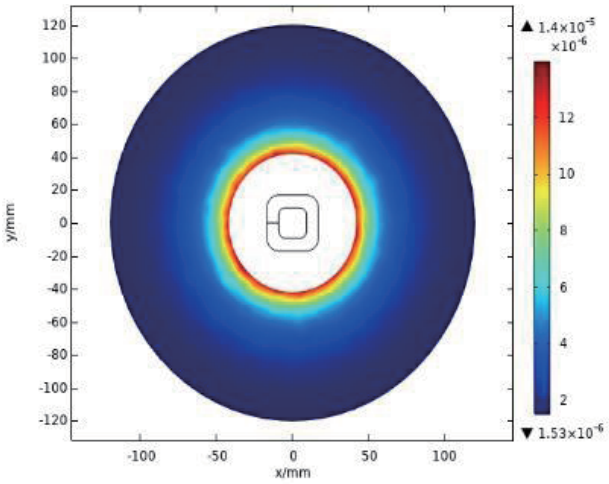

option 0

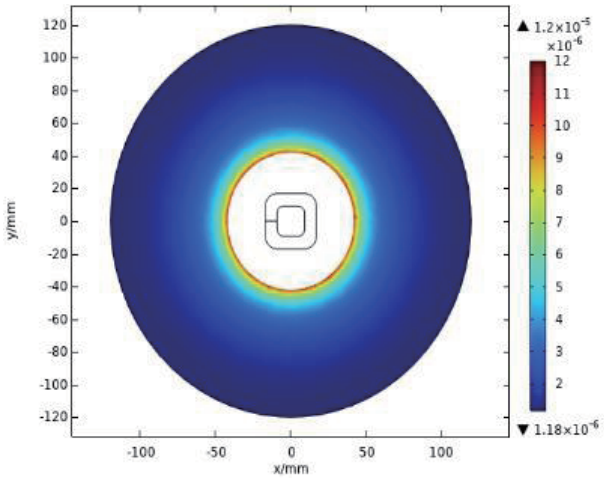

option 1

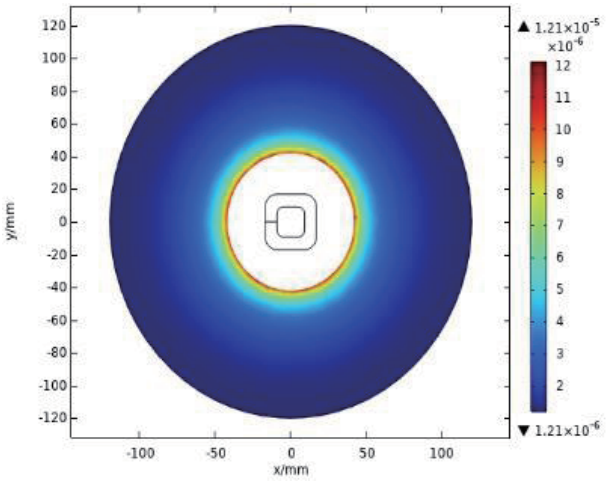

option 2

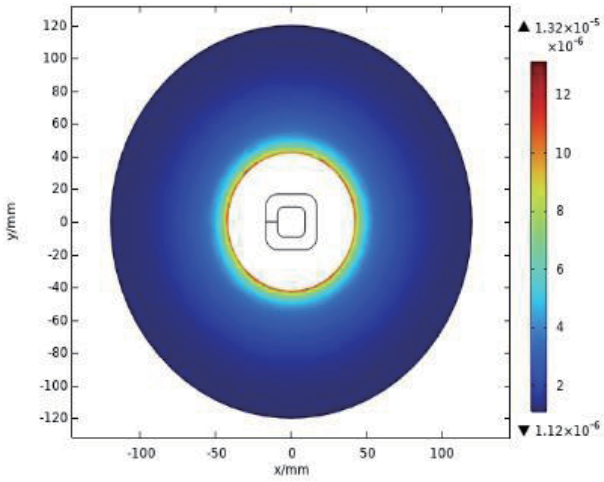

option 3

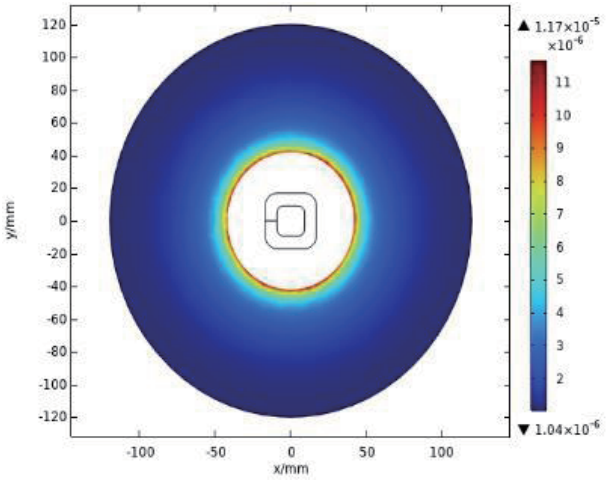

option 4

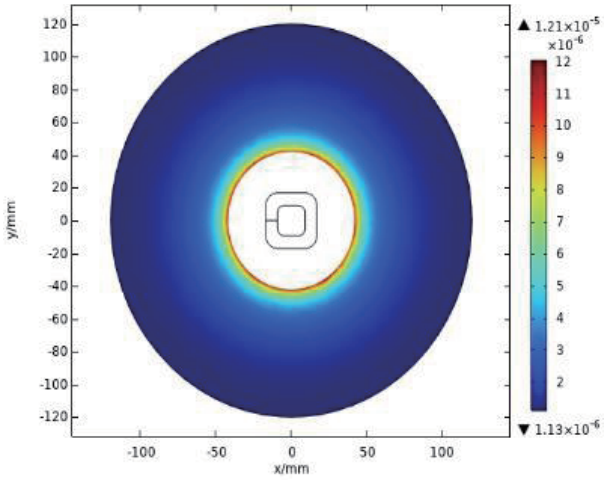

option 5

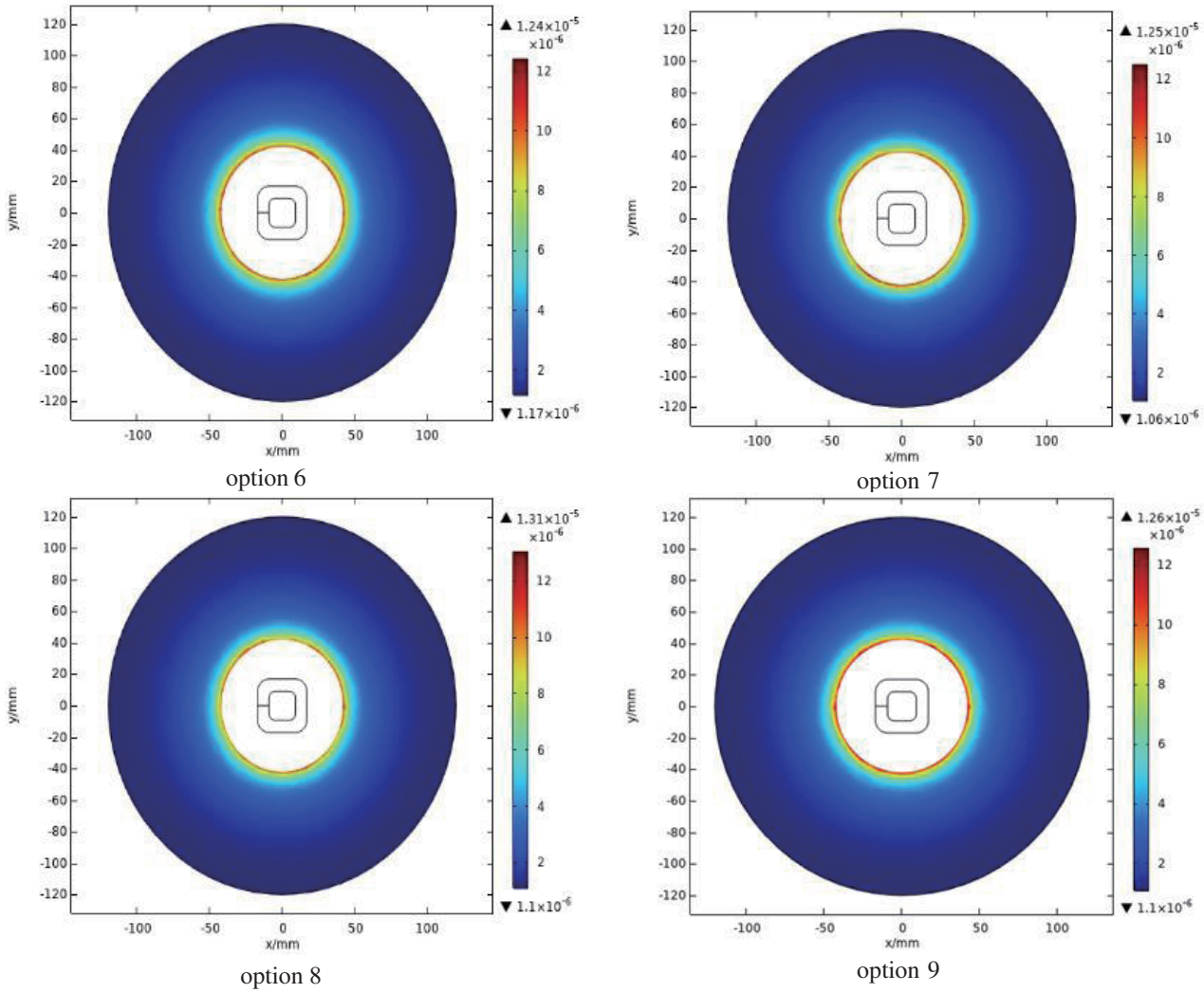

FIGURE 11. Top view comparison of magnetic flux density distribution.

TABLE 3. Comparison of transmission efficiency and magnetic field.

Set No.	Transmission efficiency (%)	Magnetic flux density at the measuring point (10^{-5} T)			
		$R_1 = 37$	$R_2 = 39$	$R_3 = 41$	$R_4 = 43$
0	88.05	1.23370	0.94993	0.80077	0.60958
1	83.86	1.03481	0.80654	0.64818	0.55012
2	83.63	1.04570	0.81537	0.66561	0.56233
3	83.21	1.13880	0.83800	0.65430	0.53684
4	86.73	0.98110	0.74723	0.58521	0.47876
5	86.35	0.99261	0.74744	0.59197	0.49178
6	86.41	0.99185	0.75766	0.60311	0.50457
7	86.66	1.09681	0.81812	0.63406	0.51231
8	86.23	1.09640	0.81817	0.64426	0.52566
9	86.32	1.12470	0.83736	0.65399	0.52392

netic leakage. However, the extent of weakening varies among the different shielding schemes.

As shown in the simulation results, in comparison to the unshielded structure, the 3-loop shielding configuration effectively diminishes the peripheral magnetic field leakage in the WPT system. The positions of magnetic field measurement points are shown in Figure 10, and Table 3 provides simulation results for magnetic field measurement points along with the system transmission efficiency. Among various shielding schemes, the 3-loop shielding coil with 7 turns and an inner

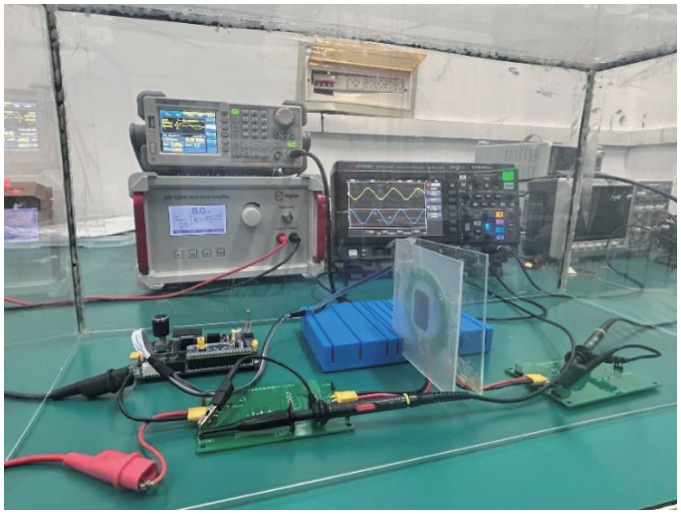

FIGURE 12. Experimental system platform.

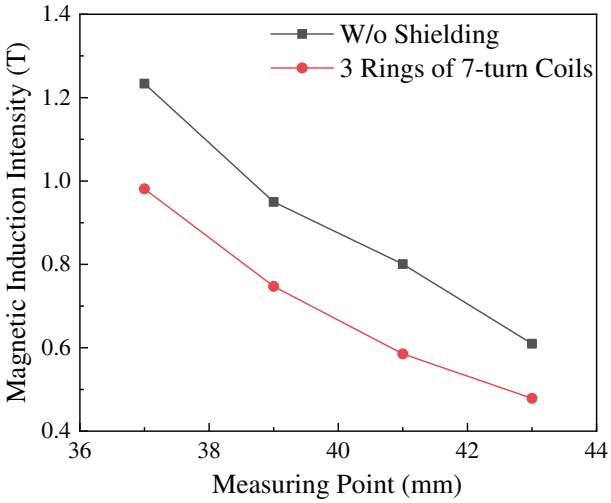

FIGURE 13. Comparison of experimental shielding effects.

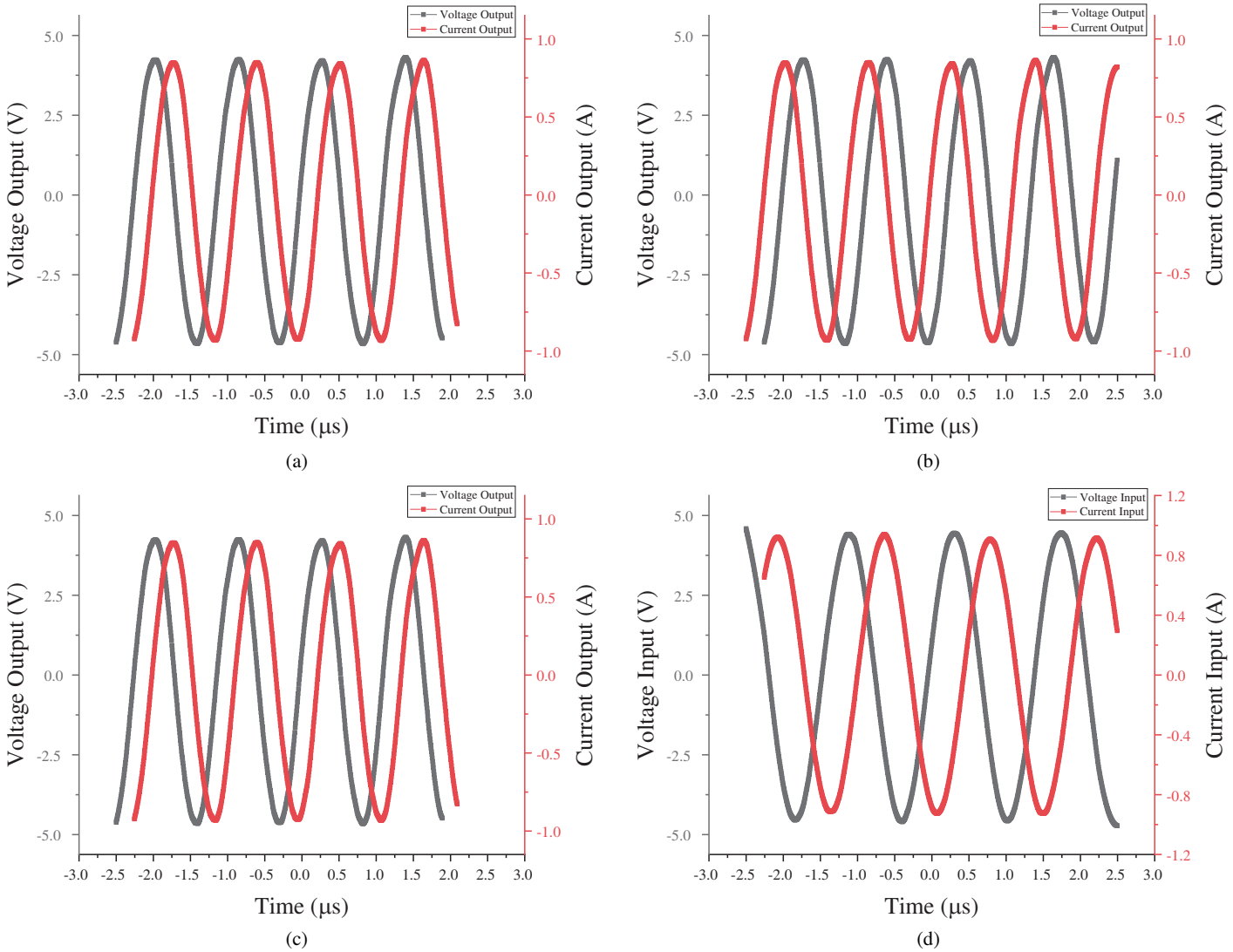

FIGURE 14. Voltage/current waveforms were collected in the experiment. (a) The unshielded structure. (b) The shielded structure.

TABLE 4. Basic parameters of each component in the system.

Parameter	Value	Parameter	Value
f/KHz	1	C_2/nF	130
L_p/μH	23	C_2/nF	6
L_s/μH	23	C_3/nF	6
L_{f1}/μH	8.58	C_4/nF	130
L_{f2}/μH	8.58		

diameter of 23 mm shows the most optimal shielding effectiveness.

4. EXPERIMENTAL VERIFICATION

4.1. The Experimental System Setup

The resonant ring multi-coil reactive shielding experimental platform is shown in Figure 12. The experimental platform consists of a power supply module, an inverter module, a primary-side compensating circuit transmitter module, a secondary-side compensating circuit receiver module, a magnetic field measurement module, and a load module. The transmitter module consists of a transmitting coil wound with copper wire and a PCB shielding coil placed parallel to its periphery. The load module simulates an 800mAh rechargeable lithium battery with a 10 Ω power resistor. The experimental platform is placed in a sealed space measuring 65 cm × 25 cm × 20 cm, constructed from 2 mm PMMA boards to prevent measurement errors caused by external environmental factors during the experiment. The basic parameters of the wireless power transfer system are presented in Table 4.

4.2. The Analysis of Experimental Results

Small electronic devices achieve wireless power transfer through magnetic coupling between coils and reduce the magnetic field leakage around the device via shielding coils. The experiment compared the magnetic field shielding effects and input-output voltage-current waveforms of the WPT system without shielding structure and the WPT system with an additional shielding structure at a transmission distance of 8 mm. The magnetic field measurement points are shown in Figure 10. The magnetic field shielding effect is illustrated in Figure 13, and the system waveforms are depicted in Figure 14. Experimental results indicate a 27.82% reduction in magnetic flux density at 41 mm from the measurement center. The system transmission efficiency decreases by only 1.32% compared to the unshielded structure, confirming the effectiveness of the resonant ring multi-coil reactive shielding structure.

5. CONCLUSION

This study aims to minimize electromagnetic leakage during the wireless charging process. A resonant ring multi-coil reactive shielding structure was designed under the resonance condition of 150 kHz. An LCC-LCC compensation circuit model was established to simulate and study the relationship between the ratio of compensating inductance to main coil inductance in the double-sided LCC circuit and the system transmission efficiency, determining the optimal compensation parameters. Simulation research on nine different turns and loop areas of shielding coils was conducted to analyze the leaked magnetic field distribution and determine the optimal structure. With the additional shielding structure, the peripheral magnetic field of the WPT system significantly decreased while ensuring system transmission efficiency.

The experimental results indicate that the reactive shielding of the multi-coil ring effectively reduces electromagnetic leakage from the periphery of the WPT system. The optimal shielding structure is identified as a 3-ring, 7-turn configuration with an inner diameter of 23 mm and an outer diameter of 35 mm. At 41 mm from the measurement center, the magnetic flux density has decreased by 27.82%, and the system transmission efficiency is only reduced by 1.32% compared to the unshielded structure.

This paper provides technical support for the study of electromagnetic shielding in the wireless power transfer process of small electronic equipment and has certain reference value.

ACKNOWLEDGEMENT

Funding information: 2023 Liaoning Provincial Department of Education Basic Research Project (General Project), Grant/Award Numbers: JYTMS20230815.

REFERENCES

[1] Yang, D., G. Xing, J. Huang, X. Chang, and X. Jiang, "QID: Robust mobile device recognition via a multi-coil qi-wireless charging system," *ACM Transactions on Internet of Things*, Vol. 3, No. 2, 1–27, 2022.

[2] Halimi, M. A., T. Khan, Nasimuddin, A. A. Kishk, and Y. M. M. Antar, "Rectifier circuits for RF energy harvesting and wireless power transfer applications: A comprehensive review based on operating conditions," *IEEE Microwave Magazine*, Vol. 24, No. 1, 46–61, 2023.

[3] Deng, S., Q. Zhang, Z. Zhuang, C. Xu, Y. Guan, and J. Dai, "Design and model of a car based on wireless charging," in *2022 6th International Conference on Robotics and Automation Sciences (ICRAS)*, 196–199, IEEE, 2022.

[4] Kuang, R. J., J. Pirakalathanan, T. Lau, D. Koh, E. Kotschet, B. Ko, and K. K. Lau, "An up-to-date review of cardiac pacemakers and implantable cardioverter defibrillators," *Journal of Medical Imaging and Radiation Oncology*, Vol. 65, No. 7, 896–903, 2021.

[5] Wang, G.-B., X.-W. Xuan, D.-L. Jiang, K. Li, and W. Wang, "A miniaturized implantable antenna sensor for wireless capsule endoscopy system," *AEU — International Journal of Electronics and Communications*, Vol. 143, 154022, 2022.

[6] Setayeshfar, O., K. Subramani, X. Yuan, R. Dey, D. Hong, K. H. Lee, and I. K. Kim, "ChatterHub: Privacy invasion via smart home hub," in *2021 IEEE International Conference on Smart Computing (SMARTCOMP)*, 181–188, IEEE, 2021.

[7] Lv, S., Z. Wei, G. Sun, S. Chen, and H. Zang, "Power and traffic nexus: From perspective of power transmission network and electrified highway network," *IEEE Transactions on Transportation Electrification*, Vol. 7, No. 2, 566–577, 2021.

[8] Dong, S., Q. D. D. Guiping, *et al.*, "Research status and development trend of electromagnetic compatibility of wireless power transmission system," *Transactions of China Electrotechnical Society*, Vol. 35, No. 13, 2855–2869, 2020.

[9] Chen, J. and Z. Liu, "Research on multi coil reactive shielding of resonant wireless energy supply cardiac pacemaker," *Transaction of China Electrotechnical Society*, Vol. 37, No. 11, 2673–2685, 2022.

[10] Lu, C., X. Huang, X. Tao, C. Rong, and M. Liu, "Comprehensive analysis of side-placed metamaterials in wireless power transfer system," *IEEE Access*, Vol. 8, 152 900–152 908, 2020.

[11] Rong, C., C. Lu, Y. Zeng, X. Tao, X. Liu, R. Liu, X. He, and M. Liu, "A critical review of metamaterial in wireless power transfer system," *IET Power Electronics*, Vol. 14, No. 9, 1541–1559, 2021.

[12] Zhou, J., P. Zhang, J. Han, L. Li, and Y. Huang, "Metamaterials and metasurfaces for wireless power transfer and energy harvesting," *Proceedings of the IEEE*, Vol. 110, No. 1, 31–55, 2022.

[13] Rong, C., L. Yan, L. Li, Y. Li, and M. Liu, "A review of metamaterials in wireless power transfer," *Materials*, Vol. 16, No. 17, 6008, 2023.

[14] Campi, T., S. Cruciani, F. Maradei, and M. Feliziani, "Magnetic field mitigation by multicoil active shielding in electric vehicles equipped with wireless power charging system," *IEEE Transactions on Electromagnetic Compatibility*, Vol. 62, No. 4, 1398–1405, 2020.

[15] Li, J., X. Huang, C. Chen, L. Tan, W. Wang, and J. Guo, "Effect of metal shielding on a wireless power transfer system," *AIP Advances*, Vol. 7, No. 5, 056675, 2017.

[16] He, X., Y. Zeng, R. Liu, C. Lu, C. Rong, and M. Liu, "A dual-band coil array with novel high-order circuit compensation for shielding design in EV wireless charging system," *IEEE Transactions on Industrial Electronics*, Vol. 71, No. 3, 2545–2555, 2024.

[17] Li, Y., K. Xie, Y. Ying, and Z. Li, "An improved hybrid shielding with LC coil for wireless power transfer system," *IEEE Transactions on Electromagnetic Compatibility*, Vol. 64, No. 3, 720–731, 2022.

[18] Kim, J. and S. Ahn, "Dual loop reactive shield application of wireless power transfer system for leakage magnetic field reduction and efficiency enhancement," *IEEE Access*, Vol. 9, 118 307–118 323, 2021.

[19] Mi, M., Q. Yang, Y. Li, P. Zhang, and W. Zhang, "Multi-objective active shielding coil design for wireless electric vehicle charging system," *IEEE Transactions on Magnetics*, Vol. 58, No. 2, 1–5, 2022.

[20] Cruciani, S., T. Campi, F. Maradei, and M. Feliziani, "Active shielding design for wireless power transfer systems," *IEEE Transactions on Electromagnetic Compatibility*, Vol. 61, No. 6, 1953–1960, 2019.

[21] Park, J., C. Park, Y. Shin, D. Kim, B. Park, J. Cho, J. Choi, and S. Ahn, "Planar multiresonance reactive shield for reducing electromagnetic interference in portable wireless power charging application," *Applied Physics Letters*, Vol. 114, No. 20, 203902, 2019.